PERFORMANCE OF HIGH-SPEED FRICTION AND WEAR OF ELECTROSPARK DEPOSITED AlCoCrFeNi HIGH-ENTROPY ALLOY COATING

C. GUO[a,d], Z. ZHAO[a], F. LU[b], B. ZHAO[c], S. ZHAO[a], J. ZHANG[a,*]
[a]School of Equipment Engineering, Shenyang Ligong University, Shenyang 110159, China
[b]North Huaan Industry Group Co. Ltd, Qiqihaer 161046, China
[c]65186 PLA Troops, Tieling 112609, China
[d]Chongqing Jianshe Industry (Group) LLC, Chongqing 400054, China

An AlCoCrFeNi high-entropy alloy coating was prepared on a CrNi3MoVA steel substrate by means of electrospark deposition (ESD) technology and its high-speed friction and wear performance investigated. The nano-mechanical properties and friction coefficient were tested by employing the nanoindentor and the friction and wear testing machine respectively, and the phase structure was obtained by using X-Ray Diffraction (XRD), and the morphologies, composition were analyzed before and after friction by utilizing scanning electron microscopy (SEM) and energy dispersive X-ray spectrum (EDS) .The results showed that the AlCoCrFeNi coating, with compact structure free of cracks, is composed of BCC and FCC double phases; the hardness of the AlCoCrFeNi coating increases about 1.0 time, the elasticity modulus reduces about 2.3%, the H/E value increases about 1.1 times, and the H^3/E^2 value increases about 7.8 times than that of the CrNi3MoVA steel; when the quenched GCr15 steel ball was used as the material of the grinding head under the friction condition that the load was 10 N, the reciprocating travel 10 millimeter and the velocity 1000 rounds per minute, the steady friction coefficient of the CrNi3MoVA steel is 0.85-0.95 while that of the AlCoCrFeNi coating only 0.29-0.38, and the wear rate of the CrNi3MoVA steel is about 9.4 times that of the AlCoCrFeNi coating. The AlCoCrFeNi coating has an obvious anti-friction and wear resistance effect, which mainly attributes to the high mechanical properties and the formed oxide scale with good adherence on the coating in the course of high-speed friction and wear.

1. Introduction

In recent years, the high-entropy alloys have attracted extensive research interests due to their unique composition, microstructure and adjustable properties. Different from traditional alloy composition, the high-entropy alloy consists of at least five principal components, and the content of each component can vary close-to-equiatomic between 5 and 35 at% or is in equiatomic percent. The high-entropy effect of high-entropy alloy favors simple stabilized solid solution structure and restrains the formation of complex phases and intermetallic compounds. The concept of the high-entropy alloy provides new methods and ideas for the development of alloy with special properties [1-2]. Up to now, many high-entropy alloys with industrial application potential have been reported, such as $Co_{1.5}CrFeNi_{1.5}Ti$ alloy with excellent wear resistance [3], AlCoCrFeNi alloy with high strength [4], $Cu_{0.5}NiAlCoCrFeSi$ alloy with outstanding corrosion resistance [5], etc. Meanwhile, the development of the high-entropy alloy is providing new quite promising materials of coating, and recently many high-entropy alloy coatings with excellent wear resistance have

---

*Corresponding author: zhangjian6165@aliyun.com

been reported, such as in situ synthesized $TiC-TiB_2/CoCrCuFeNi$ coatings by plasma transferred arc cladding (PTAC) process [6,] $CoCrFeNiW$ and $CoCrFeNiW_{0.5}Mo_{0.5}$ coatings by mechanical alloying (MA) and vacuum hot processing sintering (VHPS) technique [7], $Ni_{0.2}Co_{0.6}Fe_{0.2}CrSi_{0.2}AlTi_{0.2}$ coatings by atmospheric plasma spraying (APS) and high-velocity oxygen-fuel spraying (HVOF) process [8], etc.

The electrospark deposition (ESD) is a surface treatment technique to produce metallurgical bonded coatings with excellent performance on metallic substrate materials. In the ESD process, the electrode (anode) and the substrate (cathode) are instantaneously touched and discharged, and then the physical and chemical reactions take place in their melting pool [9]. As ESD is a simple, environment-friendly and cost-effective technology applied in many fields of industry, it gains widespread attentions and studies. The recent researches indicate that the ESD coating can increase the mechanical properties and corrosion resistance of steel [10-13], titanium alloy [14-17], nickel alloy [18] and copper alloy [19] substrates, and especially, chromium carbide-based coatings [10], $Cu/Cu-MoS_2$ self-lubricating coatings [11], WC-Co coatings [13], in-situ TiN coatings [14], CuNiSiTiZr high-entropy alloy coatings [15], Zr-based amorphous-nanocrystalline coatings [16] and Cr-Al-Si-B coatings [18] can notably improve the friction and wear performance of alloy substrate. To the best knowledge of the authors, there are still few relevant research reports on high-speed friction and wear performance of ESD high-entropy alloy coatings on steel substrate, and therefore, the high-speed friction and wear performance of an AlCoCrFeNi high-entropy alloy coatings by ESD on a CrNi3MoVA steel substrate will be investigated.

2. Materials and methods

The substrate material is $CrNi_3MoVA$ steel and its chemical composition is shown in Table 1. The bar of CrNi3MoVA steel was processed rectangle-shape samples with size of 15 mm×10 mm×3 mm, and the AlCoCrFeNi high-entropy alloy, cast by high vacuum arc melting system, was processed cylinder-shape electrode with size of Φ4 mm×50 mm by using Wire Electrical Discharge Machining (WEDM). The samples and electrode were ground using SiC abrasive paper to 800 grit finish and ultrasonically cleaned within ethanol and acetone. The AlCoCrFeNi coating was prepared by utilizing DJ-2000 type adjustable power metal surface repairing machine, and the preliminary optimized processing parameters set as outlined in Table 2.

Table 1. Chemical composition of CrNi3MoVA steel [9].

C	Mn	Si	Cr	Ni	Mo	V	S	P
0.40	0.41	0.25	1.28	3.14	0.37	0.20	0.001	0.012

Table 2. Processing parameters of ESD.

Power/W	Ar gas flow/L·min⁻¹	Electrode rotating rate/r·min⁻¹	Deposition time unit area/min·cm⁻¹
800	12	2000	2

The hardness and elasticity modulus were tested by nano indentaion G200 with Berkovich indenter and calculated by Oliver-pharr model through loading curves, and their values are the mean values of the tested eight points. The performance of high-speed friction and wear was tested by employing the HSR-2M reciprocating friction and wear testing machine. Fig. 1 shows the schematic diagram of friction and wear test. It can be seen from Fig. 1 that the material of the grinding head is a quenched GCr15 steel ball with the diameter of 4 mm, the reciprocating distance 10 mm, the reciprocating speed 1000 round per min, the load 10 N and the total friction time 5 min.
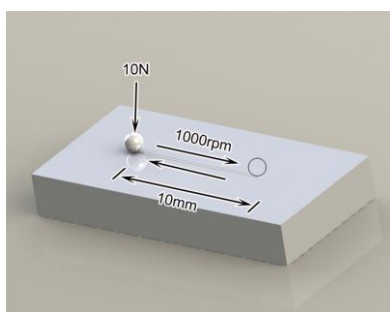
Fig. 1. Schematic diagram of friction test.

The following formula was used to test the wear resistance:

$$Wr = \frac{V}{FD}$$

(1)

where Wr is wear rate; $V = \Delta m / \rho$ is wear volume, Δm wear mass, ρ material density; F is load; D is total friction distance. The worn mass of the samples was weighed by an electronic balance (Sartorius BP211D) with a sensitivity of 10^{-5} g after ultrasonically cleaned within ethanol and acetone for 60 min.

Original and worn morphologies were obtained by scanning electron microscopy (SEM, Inspect F50, FEI Co., Hillsboro, Oregon), while the energy-dispersive spectrometer (EDS, X-Max, Oxford instruments Co., Oxford, UK) was used to analyse the chemical composition of the selected-area. The phase constitution of the coating was identified by X-ray diffraction (XRD, X' Pert PRO, PANalytical Co., Almelo, Holland).

3. Results and discussion

3.1 AlCoCrFeNi coating microstructure

Fig. 2 shows the surface morphology (a) and EDS results of area A (b) of the AlCoCrFeNi coating. The surface morphology of the AlCoCrFeNi coating presents the splashing appearance of metal (marked by the arrows) by the plasma jet at high velocity. The EDS results of area A of the AlCoCrFeNi coating as shown in Fig. 1b indicated that the composition of Al element in the coating was less than that in the electrode, which maybe for the gasification loss of Al element is bigger than that of the other four element during ESD due to its lowest boiling point as the plasma arc generated by the current pulse can reach 5000-25000 K.
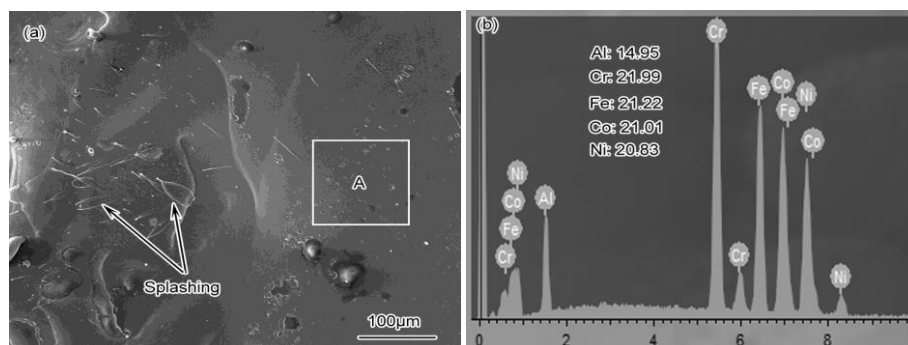
Fig. 2. Surface morphology (a) and EDS results of area A (b) of AlCoCrFeNi coating.

Fig. 3 shows the cross-section (a), magnified area B (b) morphologies and EDS line scanning (c) of the AlCoCrFeNi coating. It can be seen from Fig. 3a that there is an obvious interface line between the coating and the substrate for the substrate was corroded by 4% nital and the microstructure of the AlCoCrFeNi coating is compact and free of cracks. As shown in Fig. 3b (magnified area B in Fig. 3a), the AlCoCrFeNi coating is composed of columnar crystals with width size of less than 0.5 μm, so it belongs to the microcrystalline coating, which results from two reasons. For the first reason, the grain size of high-entropy alloy is fine and consists of nanocrystalline even in as-cast state due to high-entropy effect[1]. For the second reason, the cooling rates of the coating during ESD can attain on the order of 10^5-10^6 K/s, and in such rapid cooling speed the crystal nuclei grow up difficultly, resulting that the coating consists of microscaled and even nanoscaled structure [15]. In addition, there is an obvious melting interface (marked as the arrow) between the columnar crystals, which produced by the electrode overlapping on the last deposited coating. The EDS line scanning of the AlCoCrFeNi coating (Fig. 3c) shows that there is an element gradual transition region about 10 μm, which forms metallurgical bonding between the coating and the substrate.
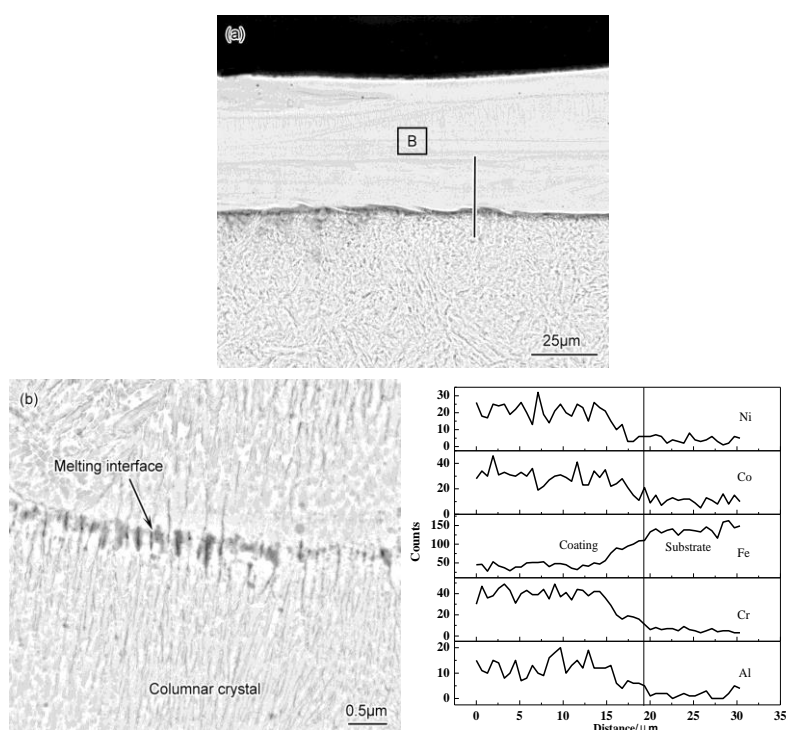
Fig. 3. Cross-section (a), magnified area B (b) morphologies and EDS line scanning c) of AlCoCrFeNi coating.

Fig. 4 shows the XRD patterns of the AlCoCrFeNi coating and electrode. As shown in Fig. 4, the AlCoCrFeNi coating is composed of BCC and FCC double phases whilst the AlCoCrFeNi electrode only consists of BCC single phase. Butler et al.[20] have investigated the effect of Al composition on the phase structure of AlCoCrFeNi high-entropy alloy by employing TEM and their results indicated that the phase structure of AlCoCrFeNi high-entropy alloy transforms from FCC+BCC (8, 10, 12, 15 (at%)) to BCC (20, 30 (at%)) when the Al content changes in the range of 8-30 (at%). In this experiment, the electrode with 20 (at%) Al content is BCC single phase while the coating with lower Al content is BCC and FCC double phases due to the ESD loss, which accords with the results of Butler et al.
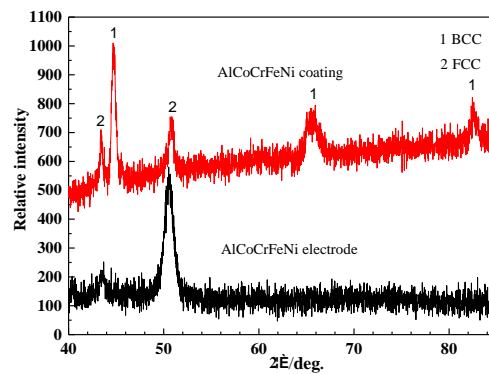
Fig. 4. XRD patterns of AlCoCrFeNi coating and electrode.

3.2 Nano-mechanical properties of CrNi3MoVA steel and AlCoCrFeNi coating

Table 3 shows the nano-mechanical properties of the CrNi3MoVA steel and AlCoCrFeNi coating. As shown in Table 3, the hardness of the AlCoCrFeNi coating increases about 1.0 time, and the elasticity modulus reduces about 2.3% than that of the CrNi3MoVA steel. The nanoindentation can also provide other significant parameters to predict the serve life of the samples. The value of H/E, a significant parameter, relates to the wear resistance of the samples [21-23] and it determines the elasticity behavior limit of the friction contact surface in the course of friction and wear. With the increase of the value of H/E, the quantity of the asperity beyond the limit of elasticity will reduce on the friction contact surface under the stress, which increase the wear resistance due to the reduced friction coefficient. As shown in Table 3, the value of H/E of the AlCoCrFeNi coating increases about 1.1 times than that of the CrNi3MoVA steel, which means that the AlCoCrFeNi coating have better wear resistance than the CrNi3MoVA steel. Moreover, the value of H^3/E^2 is another parameter in connection with wear characteristic [21-23] and it represents the capability to resist plastic deformation under the contact load, i.e. yield pressure. As shown in Table 3, the value of H^3/E^2 of the AlCoCrFeNi coating increases about 7.8 times than that of the CrNi3MoVA steel, which also indicates that the AlCoCrFeNi coating have better wear resistance than the CrNi3MoVA steel.

Table 3. Nano-mechanical properties of CrNi3MoVA steel and AlCoCrFeNi coating.

Samples	H (GPa)	E (GPa)	H/E	H^3/E^2
CrNi3MoVA steel	4.68	262.8	0.018	0.0015
AlCoCrFeNi coating	9.54	256.8	0.037	0.0132

3.3 Friction and wear behavior of CrNi3MoVA steel and AlCoCrFeNi coating

Fig. 5 shows the surface worn morphologies of low (a) and high (b) magnification, and EDS results of area C (c) and D (d) of the AlCoCrFeNi coating. As shown in Fig. 5a, the AlCoCrFeNi coating surface, distributed sporadically with some debris (marked by the arrows), is much smoother than the as-deposited coating surface. It can be seen from Fig. 5b (magnified from area C in Fig. 5a) that there are slight scratches (marked by the arrows) on the worn coating surface, which formed as the hard abrasive particles dug into the sample surface, so the wear mechanism of the AlCoCrFeNi coating is micro-cutting abrasion wear. The EDS results of area C (Fig. 5c) of the AlCoCrFeNi coating displays that the debris was oxidized for the temperature of the friction contact surface increased sharply during the process of the high-speed friction and wear. In addition, the composition of Fe element is more than the other metal element, which indicates that the debris includes the worn product of the GCr15 steel ball. The EDS results of area D (Fig. 5d) of the AlCoCrFeNi coating displays that the surface layer of the coating was also oxidized under the friction heat, and different from the as-deposited coating, the content of Al

element is much the same as other metal element in the oxidized surface layer, which indicates that the preferential oxidation of Al element happened in the high temperature. Fig. 6 shows the standard state Gibbs free energies of formation of NiO, CoO, FeO, Cr_2O_3 and Al_2O_3 as a function of temperature per mol O_2 [24]. As shown in Fig. 6, as the standard state Gibbs free energies of formation of Al_2O_3 is much less than the other oxide as a function of temperature per mol O_2, the selective oxidation of Al element in the AlCoCrFeNi coating took place at high temperature. The Al_2O_3 scale is of slow growing speed and excellent adherence, which is the main reason of outstanding oxidation resistance for the materials in high-temperature serve.
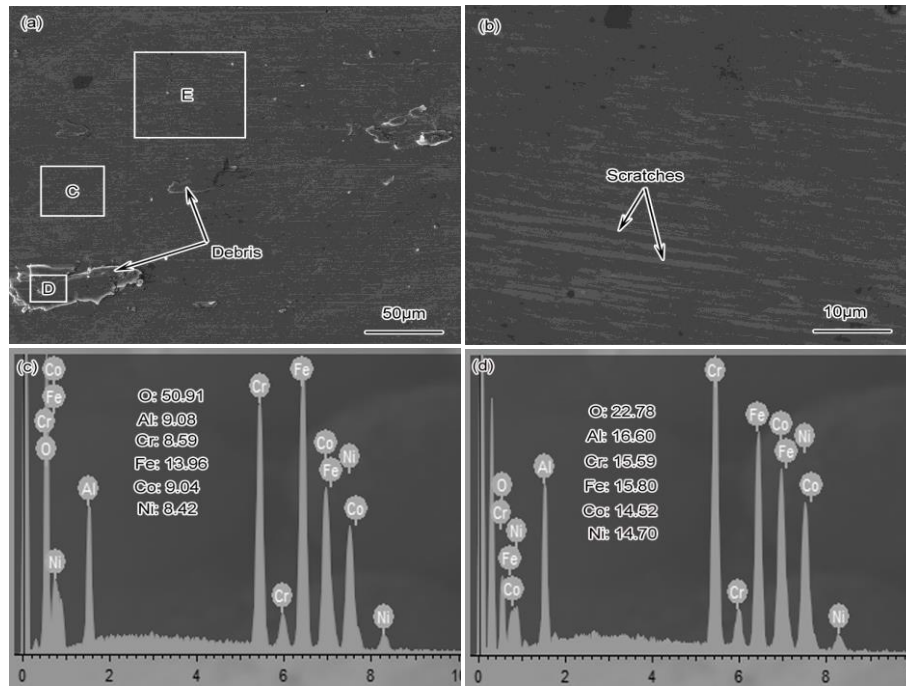
Fig. 5. Surface worn morphologies of low (a) and high (b) magnification, and EDS results of area C (c) and D (d) of AlCoCrFeNi coating.
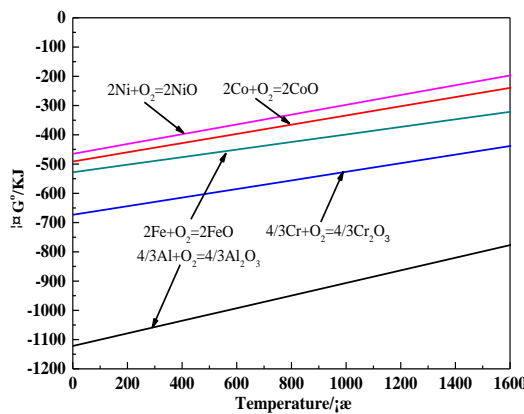
Fig. 6. Standard state Gibbs free energies of formation of NiO, CoO, FeO, Cr_2O_3 and Al_2O_3 as a function of temperature per mol O_2.

Fig. 7 shows the surface worn morphologies of low (a) and high (b) magnification, and EDS results of area G (c) and H (d) of the CrNi3MoVA steel. As shown in Fig. 7a, different from the morphologies of the AlCoCrFeNi coating, there is a mass of wear debris aggregation (marked as the arrows) on the worn surface of the CrNi3MoVA steel, which is a typical morphology of

adhesive wear, in which the shear damage of the adhesive contacting points occurs in the shallow layer and the sheared metal smears at the interface of the friction pair. It can be seen from Fig. 7b (magnified from area F in Fig. 7a) that much small debris gets together to form the debris aggregation, around which chunks of debris piles up. The EDS results of area G (Fig. 7c) of the CrNi3MoVA steel shows that the debris aggregation consists of ferric oxides, which indicates that the debris at the interface of the friction pair oxidized at high temperature caused by the high-speed friction and wear. The ferric oxides have high hardness, for example, the microhardness of Fe_2O_3 is 1000 HV, and they would dig into the sliding sample surface and lead to the intense plastic formation of the metal between the friction pair to produce long continuous parallel furrows on the steel surface (marked as the arrows), which would aggravate the wear of the CrNi3MoVA steel. The EDS results of area H (Fig. 7d) uncovered with debris shows that this area only consists of the elements of the CrNi3MoVA steel indicating there is no oxide scale on the steel surface. Thus, the wear mechanism of the CrNi3MoVA steel mainly belongs to severe adhesive and abrasion wear.
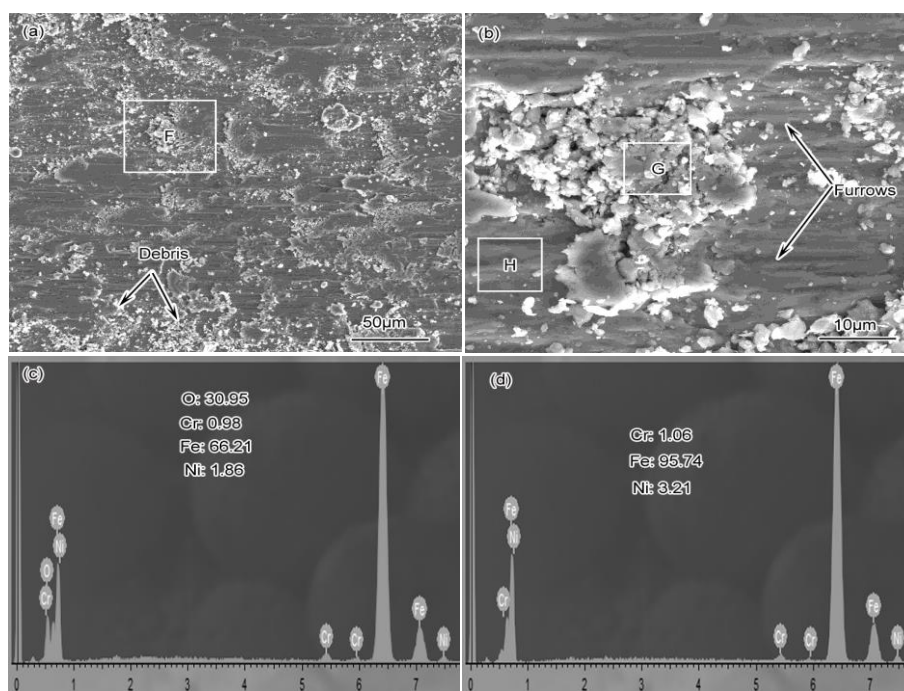
Fig. 7. Surface worn morphologies of low (a) and high (b) magnification, and EDS results of area G (c) and H (d) of CrNi3MoVA steel.

Fig. 8 shows the friction coefficient and wear rate of the CrNi3MoVA steel and AlCoCrFeNi coating. As shown in Fig. 8a, the steady friction coefficient of the CrNi3MoVA steel is 0.85-0.95 while that of the AlCoCrFeNi coating only 0.29-0.38, so the AlCoCrFeNi coating has an obvious anti-friction effect. It can be seen from Fig. 8b that the wear rate of the CrNi3MoVA steel is 8.6×10^{-4} mm^3/(N·m) whilst that of the AlCoCrFeNi coating only 9.15×10^{-5} mm^3/(N·m), and the wear rate of the CrNi3MoVA steel is about 9.4 times that of the AlCoCrFeNi coating.
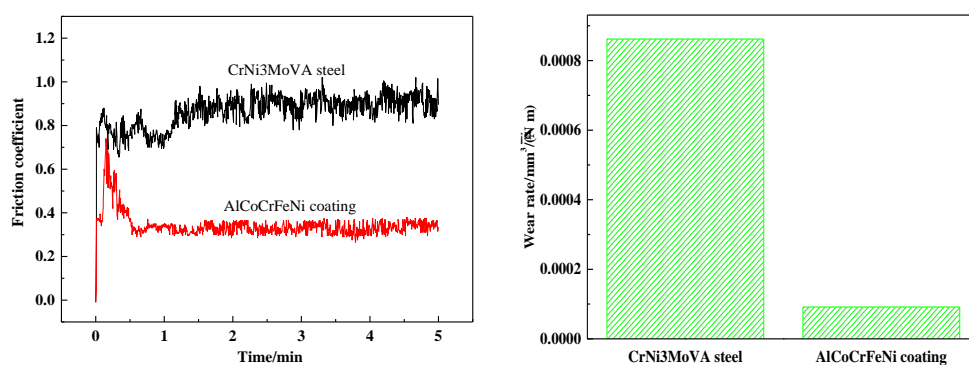
Fig. 8. Friction coefficient and wear rate of CrNi3MoVA steel and AlCoCrFeNi coating.

The performance of high-speed friction and wear of the AlCoCrFeNi coating has an remarkable increase in contrast to that of the CrNi3MoVA steel. For the first reason, the AlCoCrFeNi coating has outstanding mechanical properties that include high hardness, H/E and H^3/E^2 values. For the second reason, the oxide scale formed on the AlCoCrFeNi coating during the high-speed friction and wear has excellent adherence and can play a role of self-lubricating, so the AlCoCrFeNi coating has much lower friction coefficient. W. L. Li et al. [25] have also proposed that the oxide scale formed on the metal is beneficial for the increase of the metal wear resistance. The ESD AlCoCrFeNi coating belongs to microcrystalline coating with columnar crystal structure. On the one hand, the columnar crystal is the rapid diffusion channel of the ion and makes oxide nucleate preferentially; on the other hand, the microcrystalline coating consists of more grain boundaries, which can be as the preferential nucleation sites and the rapid diffusion channel of the ion [26-27].

4. Conclusions

1) The ESD AlCoCrFeNi coating with compact microstructure is composed of BCC and FCC double phases.

2) The hardness of the AlCoCrFeNi coating increases about 1.0 time, the elasticity modulus reduces about 2.3%, the H/E value increases about 1.1 times, and the H^3/E^2 value of the AlCoCrFeNi coating increases about 7.8 times than that of the CrNi3MoVA steel.

3) The steady friction coefficient of the CrNi3MoVA steel is 0.85-0.95 while that of the AlCoCrFeNi coating only 0.29-0.38, and the wear rate of the CrNi3MoVA steel is about 9.4 times that of the AlCoCrFeNi coating, and the AlCoCrFeNi coating has an obvious anti-friction and wear resistance effect.

4) The mechanism of the CrNi3MoVA steel can be characterized as severe adhesive and abrasion wear while that of the AlCoCrFeNi coating is micro-cutting abrasion one, and the better high-speed performance of the AlCoCrFeNi coating results from the high mechanical properties and the formed oxide scale with good adherence on the coating in the course of high-speed friction and wear.

References

[1] Y. Zhang, T. T. Zuo, Z. Tang, Z. Tang, M. C. Gao, K. A. Dahmen, P. K. Liaw, Z. P. Lu, Progress in Materials Science **61**(8), 1(2014).

[2] X. R. Wang, Z. Q. Wang, T. S. Lin, P. He, Journal of Materials Processing Technology **241**, 93 (2016).

[3] M. H. Chuang, M. H. Tsai, W. R. Wang, S. J. Wang, J. W. Yeh, Acta Materialia **5916**, 6308 (2011).

[4] Y. Zhang, B. Zhang, K. Li, G. L. Zhao, S. M. Guo, Journal of Alloys & Compounds **734**, 220 (2017).

[5] Y. Y. Chen, T. Duval, U. D. Hung, J. W. Yeh, H. C. Shih, Corrosion Science **47**(9), 2257 (2005).

[6] J. B. Cheng, D. Liu, X. B. Liang, Y. X. Chen, Surface & Coatings Technology **281**(7), 109 (2015).

[7] C. Y. Shang, E. Axinte, J. Sun, X. T. Li, P. Li, J. W. Du, P. C. Qiao, Y. Wang, Materials & Design **117**, 193 (2017).

[8] W. L. Hsu, H. Murakami, J. W. Yeh, A. C. Yeh, K. Shmioda, Surface & Coatings Technology, **316**, 71 (2017).

[9] J. B. Yang, Y. C. Wang, J. H Qu, Q. P. Guo, H. Jin, J. Zhang, Materials Review **31**, 51 (2017).

[10] K. Korkmaz, Surface and Coatings Technology 272, 1 (2015).

[11] T. K. Cao, S. Lei, M, Zhang, Surface and Coatings Technology **270**, 24 (2015).

[12] N. I. Jamnapara, S. Frangini, J. Alphonsa, N. L. Chauhan, S. Mukherjee, Surface and Coatings Technology **266**(3), 146 (2015).

[13] A. A. Burkov, S. A. Pyachin, Materials & Design **80**, 109 (2015).

[14] X. Hong, Y. F. Tan, X. L. Wang, H. Tan, T. Xu, Transactions of Nonferrous Metals Society of China **25**, 3329 (2015).

[15] X. R. Wang, Z. Q. Wang, P. He, T. S. Lin, Y. Shi, Surface and Coatings Technology **283**, 156 (2015).

[16] X. Hong, Y. Tan, C. Zhou, X. Ting, Z. W. Zhang, Applied Surface Science **356**, 1244 (2015).

[17] Y. Liu, D. Wang, C. Deng, L. X. Huo, L. J. Wang, R. Fang, Journal of Alloys Compounds **628**, 208 (2015).

[18] A. E. Kudryashov, A. Y. Potanin, D. N. Lebedev, I. V. Sukhorukova, D. V. Shtansky, E. A. Levashov, Surface and Coatings Technology **285**, 278 (2015).

[19] P. Luo, S. J. Dong, A. Yangli, S. X. Sun, Z Zheng, H. H. Wang, Journal of Asian Ceramic Societies 3(1), 103 (2015).

[20] T. M. Buter, M. L. Weaver, Journal of Alloys & Compounds **674**, 229 (2016)

[21] J. Cheng, D. Liu, X. Liang, Y. X. Chen, Surface & Coatings Technology **281**(7), 109 (2015).

[22] A. Leyland, A. Matthews, Wear 246(1), 1 (2000).

[23] L. Ipaz, J. C. Caicedo, J. Esteve, F. J. Espinoza-beltran, G. Zambrano, Applied Surface Science **258**(8), 3805 (2012).

[24] Y. J. Liang, Y . C. Che, Handbook of Inorganic Compound of Thermodynamic Data, 1nd ed., Northeastern University, Shenyang 1993, 450

[25] W. L. Li, N. R. Tao, Z. Han, Wear **274-275**, 306 (2012).

[26] H. Y. Lou, F. H. Wang, B. J. Xia, L. X. Zhang, Oxidation of Metals **38**(3-4), 299 (1992).

[27] J. L. Wang, M. H. Chen, Y. X. Cheng, L. L. Yang, Z. B. Bao, L. Liu, S. L. Zhu, F. H. Wang, Corrosion Science **123**, 27 (2017).